nature electronics

Supplementary information

https://doi.org/10.1038/s41928-026-01662-9

Parallel enzymatic DNA synthesis using a semiconductor chip

In the format provided by the authors and unedited

Contents

Work	Synthesis chemistry	Parallelization method	Synthesis metric		
			No. distinct sequences	Length, total (nt)	Length, feature sequence (nt)
This work	Enzymatic	Electrode array (CMOS)	1	102	79
			64	38–39	10–11
Ref. 17		Electrode array (CMOS)	1	1	n/a
Ref. 16		Electrode array	1	1	n/a
Ref. 4		Inkjet printing	3	50	50
Ref. 10		Photolithography	12	8 cycles	8 cycles
Ref. 18, 19	Phosphoramidite	Electrode array (CMOS)	~10^7	170	n/a
Ref. 3		Inkjet printing	~10^6	300	n/a
			~10^6	150–154	~110
Ref. 9		Photolithography	~10^6	100	100

Supplementary Table 1 | Comparison of parallel DNA synthesis platforms. In cases where total length and feature sequence length match, primers are not synthesized and no NGS is performed. Since Ref. 10 lacks single-base resolution (*i.e.*, in a given cycle, the elongation is done with multiple bases of same type), cycle count is presented instead of length.

Bulk deprotection

Position	A (%)	T (%)	C (%)	G (%)
1	0.0	99.8	0.0	0.2
2	0.7	0.3	0.0	99.0
3	0.1	99.4	0.2	0.3
4	0.4	0.5	0.1	99.0
5	0.1	99.4	0.2	0.3
6	0.2	0.2	99.5	0.1
7	99.6	0.1	0.2	0.2
8	0.3	0.3	0.1	99.4
9	99.4	0.1	0.3	0.2
10	0.1	0.4	99.1	0.3
Consensus sequence			**TGTGTCAGAC**	

Electrochemical deprotection

Position	A (%)	T (%)	C (%)	G (%)
1	0.2	99.4	0.2	0.2
2	0.3	1.9	0.2	97.6
3	0.3	1.3	96.6	1.8
4	0.2	0.3	97.8	1.7
5	0.2	99.3	0.4	0.2
6	0.2	0.9	1.2	97.7
7	1.8	96.9	0.6	0.7
8	0.4	0.3	97.9	1.3
9	1.3	0.3	98.2	0.2
10	0.3	98.2	1.3	0.2
Consensus sequence			**TGCCTGTCCT**	

Supplementary Table 2 | Percentages of base reads at each nucleotide position after Filter 2 for the 10-nt single sequence synthesis runs in Fig. 3. The data are presented here for both bulk and electrochemical deprotection methods.

Feature-sequence length	Full-length purity	Error per nucleotide				Coupling efficiency
		Deletion	Insertion	Substitution	Total	
10 nt	52.8%	8.20%	0.26%	1.17%	9.63%	93.8%
29 nt	28.3%	13.62%	0.63%	0.34%	14.59%	96.0%
59 nt	9.7%	22.77%	0.50%	0.77%	24.04%	96.2%
79 nt	2.2%	38.18%	3.12%	0.88%	42.18%	95.3%

Supplementary Table 3 | Raw feature-sequence synthesis errors in NGS reads (after Filter 1) for single-sequence syntheses with varying feature-sequence lengths on the 256-pixel CMOS chip (see Fig. 3).

64-sequence synthesis	Full-length purity	Error per nucleotide				Coupling efficiency
		Deletion	Insertion	Substitution	Total	
10–11-nt feature sequence	18.7%	26.2%	1.0%	6.0%	33.2%	84.6%
7–8-nt feature sequence	26.4%	22.0%	1.9%	7.9%	31.8%	83.9%
7–8-nt feature sequence	22.5%	25.3%	2.5%	7.4%	35.3%	82.1%

Supplementary Table 4 | Raw feature-sequence synthesis errors in NGS reads (after Filter 1) for three runs of parallel 64-sequence synthesis. In the last two runs, sequence-to-pixel assignments are shuffled. See Fig. 4 (first run) and Extended Data Fig. 2 (second and third runs) for experimental context and setup. All error percentages are averaged over pixels; for pixel-resolved maps, see Extended Data Fig. 3 (first run) and Supplementary Figure 9 (second and third runs).

Number of sequences	Pixel pitch (μm)	Length, total (nt)	Length, feature sequence (nt)	Correct length ratio after Filter 2	Correct consensus ratio after Filter 3	Sequence-recovery error
64	160	35–36	7–8	64/64	64/64	0%
64	160	35–36	7–8	64/64	64/64	0%
64	160	38–39	10–11	64/64	61/64	1.9%
64	160	38–39	10–11	40/64	40/64	10.1%
64	160	38–39	10–11	44/64	42/64	13.8%
200	80	34	6	128/200	81/200	-

Supplementary Table 5 | Synthesis fidelity across multi-sequence runs on the 256-pixel CMOS chip. Summary of error metrics for multi-sequence synthesis runs at varying pixel pitch and target length. Correct-length ratio (after Filter 2): fraction of sites whose representative (most-frequent) feature length equals the target feature length. Correct-consensus ratio (after Filter 3): fraction of sites whose per-site consensus feature sequence matches the target feature sequence. Sequence-recovery error: per-base error in recovered consensus sequences. For entries 1–2, see Extended Data Fig. 2 and Supplementary Figure 9; for entry 3, see Fig. 4 and Extended Data Fig. 3; for entry 6, see Fig. S11. Entries 4–5 encountered systematic issues during synthesis; entry 4 reflects chip damage from post-fabrication/packaging, and entry 5 experienced mid-run depletion of elongation solution that introduced deletion errors before resuming. In addition, entry 5 used a higher injected current (±79.0 nA) to localize a lower pH (~5.1) than the pH ~ 5.3 used elsewhere on the 256-pixel CMOS chip.

21-nt feature sequence	Full-length purity	Error per nucleotide				Coupling efficiency
		Deletion	Insertion	Substitution	Total	
e13	42.8%	2.34%	0.32%	0.91%	3.56%	96.0%
e8	36.8%	2.97%	0.28%	0.7%	3.95%	95.3%
q4	34.3%	3.04%	0.24%	0.67%	3.94%	95.0%

Supplementary Table 6 | Raw feature-sequence synthesis errors in NGS reads for the three sequences synthesized on the 4-pixel chip (Supplementary Figure 12b). Error rates represent analysis of the feature region only, obtained by aligning NGS reads to the full reference (seed oligo + feature + primer) and extracting errors within the feature sequence.

Feature sequence length	Full-length purity	Error per nucleotide				Coupling efficiency
		Deletion	Insertion	Substitution	Total	
21 nt	50.3%	3.47%	0.11%	0.31%	3.88%	96.8%
31 nt	41.5%	3.12%	0.16%	0.15%	3.43%	97.2%
51 nt	22.0%	4.47%	0.10%	0.29%	4.86%	97.1%
71 nt	14.7%	4.32%	0.16%	0.24%	4.71%	97.3%

Supplementary Table 7 | Raw feature-sequence synthesis errors in NGS reads for single-sequence syntheses of varying feature-sequence lengths on the 4-pixel chip. Error rates represent analysis of the feature region only, obtained by aligning NGS reads to the full reference (seed oligo + feature + primer) and extracting errors within the feature sequence.

Array size	DNA length	Operational parameters for synthesis (per run)				Pixel pitch	Pixel no.	Feature sequence length	Data volume	Cost (per TB)
		Cycle	Time	Expense	Waste					
10 × 10 cm^2	200 nt	588	114 h	$11,290 (reagent)	7,056 mL	30 μm	1.1×10^7	162 nt	0.36 GB	$31M
						1 μm	10^{10}	156 nt	310 GB	$36k
						100 nm	10^{12}	152 nt	30 TB	$376
						10 nm	10^{14}	147 nt	2.94 PB	$3.8

Supplementary Table 8 | Scenario analysis of synthesis cost scaling with parallelism. This table analyzes how synthesis cost scales with pixel pitch (and thus pixel count), assuming that the present deprotection-chemistry constraints are removed. We fix: 200-nt total length per pixel on a 10 × 10 cm^2 array with a ~100 μm microfluidic gap; 588 cycles (~114 hours; greedy algorithm); $11,290 total synthesis-reagent cost; and ~7 L aqueous waste — all independent of pixel pitch. These fixed values follow because the reagent volume per cycle is set by the chip area and the microfluidic gap; the $11,290 figure is calibrated from the volume-cost relationship of a commercial enzymatic system (Simmons *et al.*, *Front. Bioeng. Biotechnol.* 2023). Data capacity (here using 1.6 bit/nt) then scales primarily with pixel count, *i.e.*, with the inverse square of the pixel pitch, with a minor adjustment from ID length (200 nt includes feature sequence (or payload in the context of data storage) plus ID/primer/error-correction; ID grows only logarithmically with pixel count and thus only slightly nudges feature sequence and total data). As shown, at a 30-μm pixel pitch (~1.1×10^7 pixels), capacity is ~0.36 GB, giving a normalized cost of ~$31 M/TB; at a 100-nm pixel pitch (~10^{12} pixels), capacity is ~30 TB with a normalized cost of ~$376/TB. These figures illustrate how a fixed synthesis cost per run for a given chip area and target length is amortized over more data as pitch shrinks. Of note, although leading-edge CMOS technology affords sub-3-nm transistor features, achieving the 100-nm pixel (concentric ring pair) pitch is ambitious. The fine metallic wiring that could support such pitch lies deep under the passivation; using it as electrodes would require opening the passivation. Also at advanced nodes, internal wiring is copper in fragile dielectrics, which is not robust to electrolyte exposure (corrosion), necessitating capping with a noble metal, which could inflate the pitch. Thus, the 100-nm (and finer) entries should be read as directional scaling points, not immediate targets.

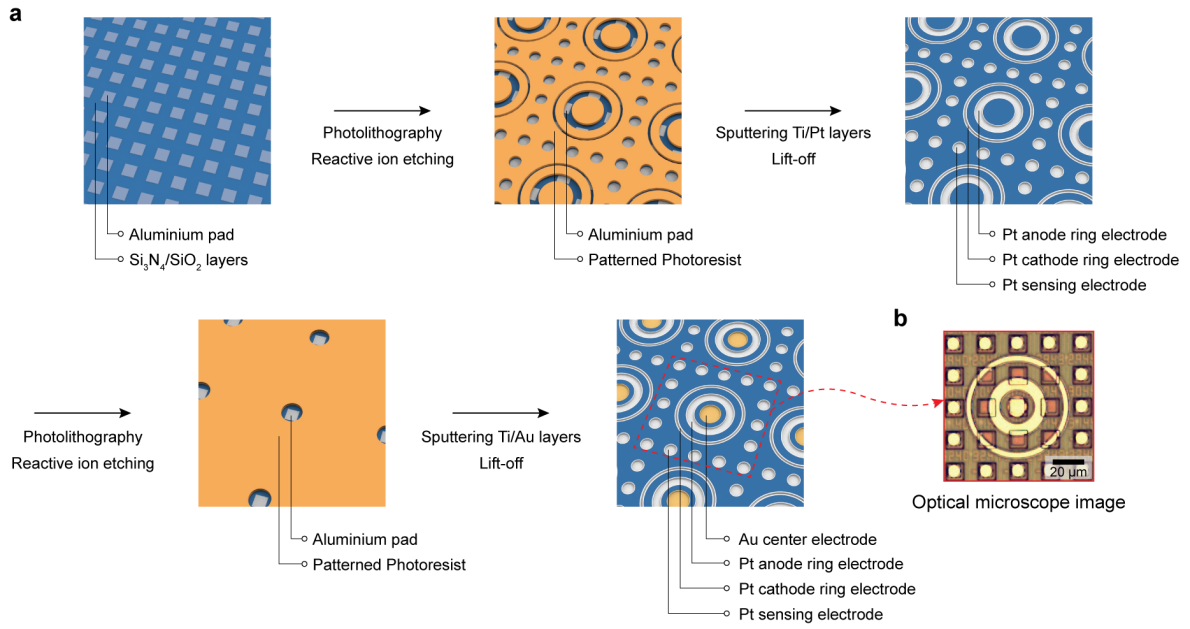

Supplementary Figure 1 | Structure of, and post-fabrication steps for, the 16 × 16 = 256 electrochemical pixel array on the CMOS chip. Our CMOS chip, in its foundry-fabricated form, features an array of 64 × 64 = 4,096 aluminum (Al) pads on the surface, covered by a SiO_2/Si_3N_4 passivation layer. Each pad has a dimension of 10.5 × 10.5 μm^2 and the pad-to-pad (center-to-center) pitch is 20 μm. Each pad is connected to its own circuit in the underlying CMOS chip (all 4,096 pad circuits are identical). Each pad circuit can be configured into a galvanostat that can inject a current, a potentiostat that can apply a voltage, or an amplifier that can measure OCP. It is on this pre-defined array of 64 × 64 = 4,096 Al pads that we post-fabricate the array of 16 × 16 = 256 concentric platinum (Pt) electrode ring pairs as electrochemical pixels, together with gold (Au) pixel center electrodes and peripheral Pt electrodes in between pixels. As shown in part **b**, after the post-fabrication, the inner Pt ring of a pixel is connected to 4 Al pads, the outer Pt ring of the pixel is connected to another 4 Al pads, the pixel center Au electrode is connected to 1 Al pad, and each peripheral electrode is connected to 1 Al pad. The 4 pad circuits connected to the inner (or the outer) ring are configured into galvanostats or current injectors and are operated together as one effective current injector. The pad circuit connected to a peripheral Pt electrode is configured into an amplifier to measure OCP. The pad circuit connected to a pixel center Au electrode is not used during synthesis, but is configured into a potentiostat that can apply a voltage during cyclic voltammetry to electrodeposit Au nanostructures onto the Au pixel center electrode. The post-fabrication steps are as follows (part **a**): (1) photolithography to define the patterns for the concentric electrode rings and peripheral electrodes; (2) reactive ion etching (RIE) to remove the passivation layer to expose the Al pads; (3) deposition of a metal layer (20 nm titanium (Ti) followed by 200 nm Pt) via sputtering, and lift-off to remove the photoresist; (4) photolithography to define the pattern for the Au pixel center electrodes; (5) deposition of a metal layer (20 nm Ti followed by 200 nm Au) via sputtering, and lift-off.

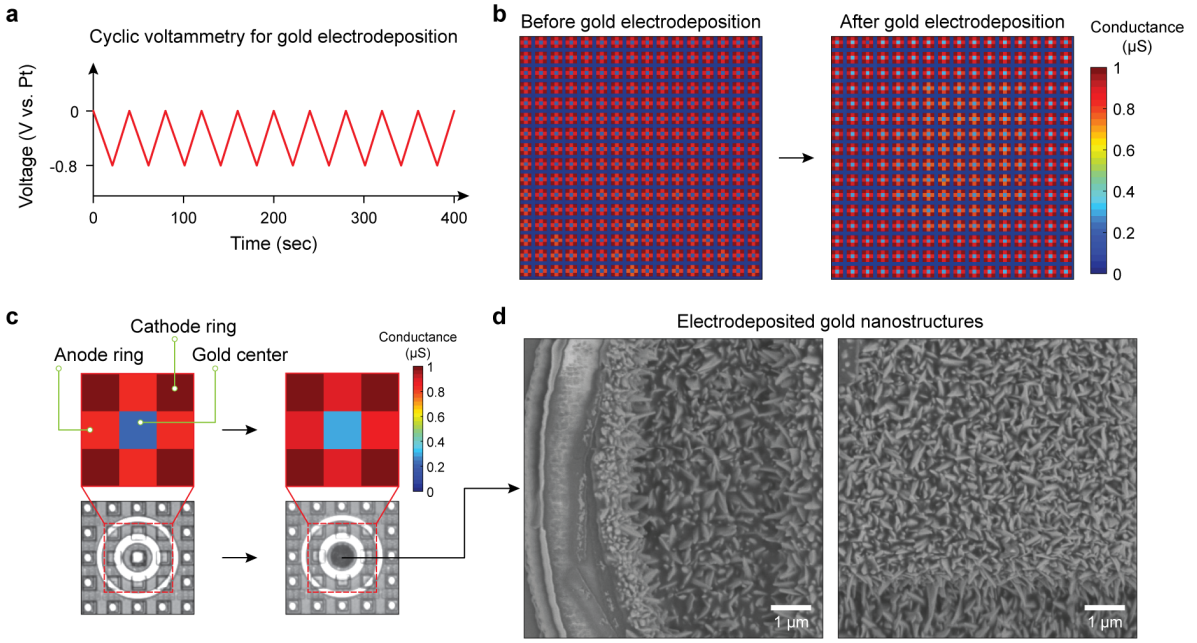

Supplementary Figure 2 | Electrodeposition of gold nanostructures. Gold nanostructures are electrodeposited on the pixel center gold electrodes to increase their surface area and thus the amount of thiolated seed oligos grafted therein. The gold center electrode within each pixel of the 256-pixel array has a diameter of ~8 μm as post-fabricated, which increases to ~19 μm after gold nanostructure electrodeposition, enlarging the seeding area. For the electrodeposition, we run cyclic voltammetry (CV) for 10 cycles, with the voltage repeatedly scanned between 0 V and –0.8 V at a rate of 40 mV/s (part **a**). The electrodeposition solution is 1X PBS containing 5 mM $HAuCl_4$. The electrodeposition is evidenced by the increase of the conductance of the pixel center gold electrodes (part **b**: array-wide view; part **c**, top; close-up view), or by the darkness appearance for the gold center electrode in optical imaging (part **c**, bottom). Part **d** shows SEM images of the electrodeposited gold nanostructures.

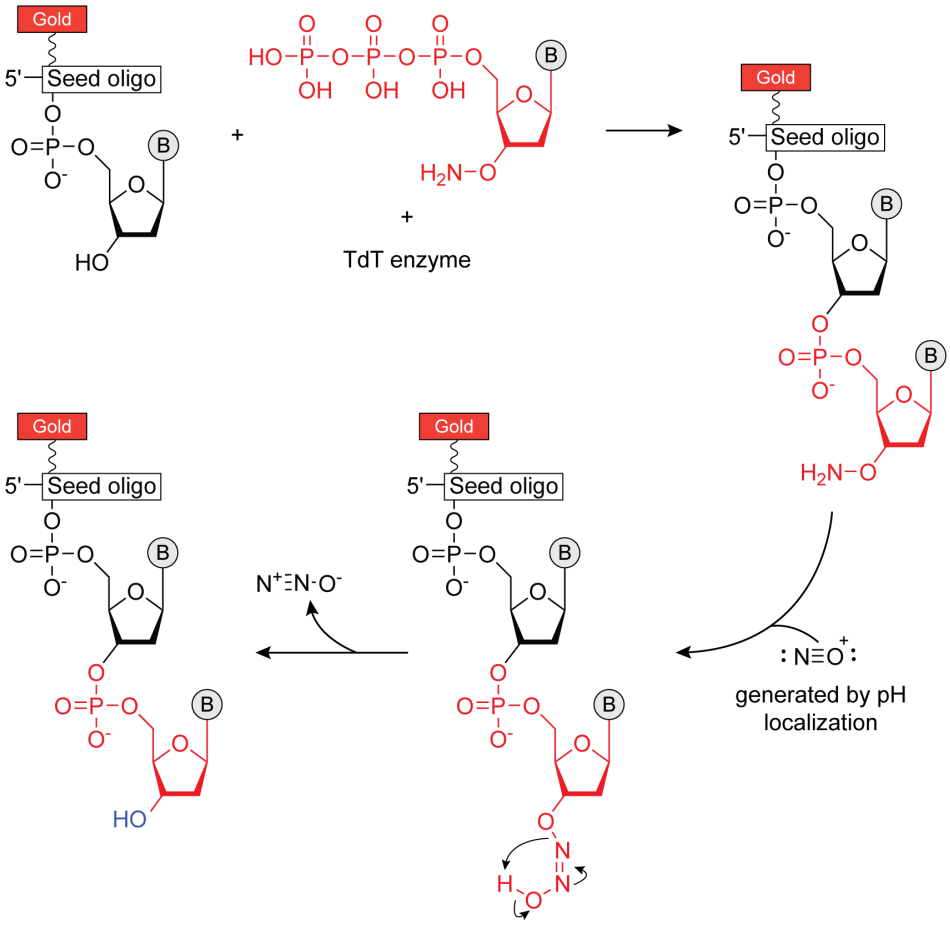

Supplementary Figure 3 l Plausible DNA deprotection mechanism in an acidic environment. While the exact mechanism underlying the deprotection of 3´-aminooxy protected DNA molecules in an acidic environment is unknown, one plausible mechanism is as follows. Our quinone solution contains nitrite ions, and in an acidic environment, these nitrite ions are protonated to generate nitrous acid, which are subsequently protonated to yield nitrosonium ions (NO^+). These nitrosonium ions may act as electrophiles to convert the 3´-aminooxy groups into 3´-hydroxyl groups in the DNA molecules, leading to their deprotection.

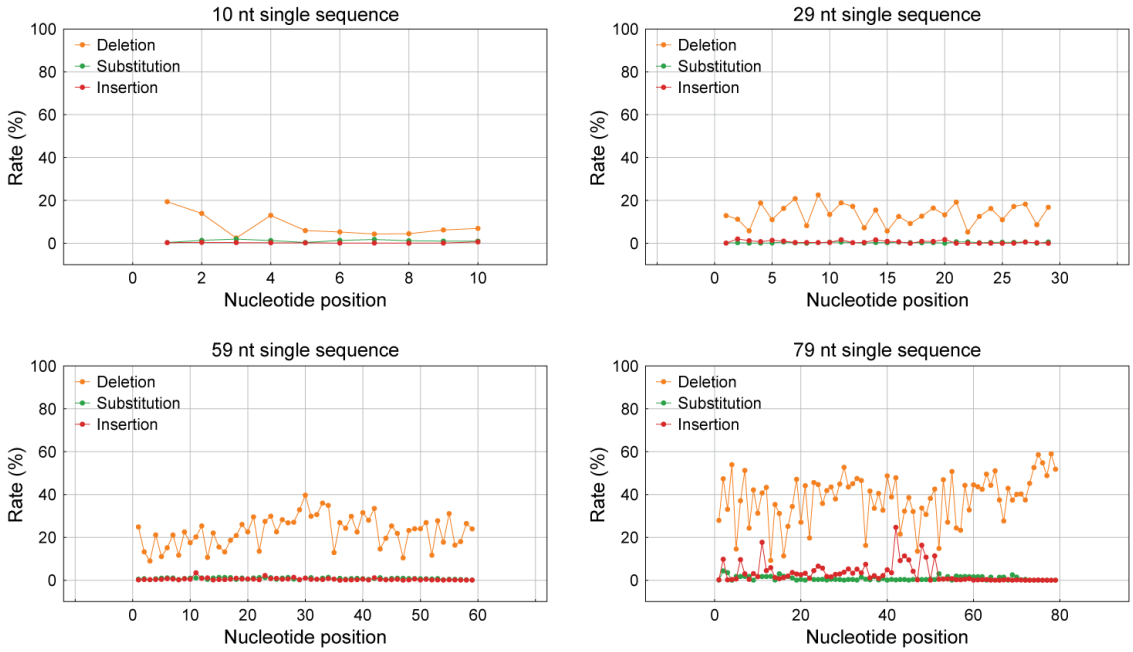

Supplementary Figure 4 | Per-nucleotide error profiles in the feature sequence for single-sequence synthesis (after Filter 1). For each error-type—deletion, substitution, and insertion—, the per-nucleotide error rate is plotted along the feature-sequence position for four lengths (10, 29, 59, and 79 nt). See Fig. 3 for experimental context and setup.

a

TTTATTGTGATGAAGC
TTTGTAAGTAAGACAG
TTTCTGAAGCGAGTAA
TTATTCATAGGAAGCC
TTAATAGCGTGTTAGG
TTAGTAACTCTGTTAG
TTACTCAAGCCACTGA
TTGTTGAATGTTAGGA
TTGATAGCAACTTAGC
TTGGTCACTGACATAG
TTGCTTAAGCGACATT
TTCTTGTTACATAGGT
TTCATAGTAAGCGTGT
TTCGTTAGGCAGCGAG
TTCCTCCACACAGCTA
TATTTGAAAGATAGAC
TATATAGAATGCGTGT
TATGTTATAGAGCCAC
TATCTTGTGTTAGGCA
TAATTGCGAGCCACAC
TAAATAGCTAGAAAGA
TAAGTTAGACAGAATG
TAACTTTAGGAACTCT
TAGTTGTTAGCTAGGA
TAGATAGCAAGGAACA
TAGGTTAGAAAGATTG
TAGCTCTTGTTACACA
TACTTGGTAGAAACTG
TACATAGAAAGTAACT
TACGTCTGTTAGGAAG
TACCTCAAGTAAGACA
TGTTTGGAAGCGAGTA
TGTATACATAGGAAGC
TGTGTCAGCGTGTTAG
TGTCTAAAGCAAGTGA
TGATTCTGAGTAAGTC
TGAATAGAAACTCTG
TGAGTTTACATAGGT
TGACTAGAATGTTAG
TGGTTAAAGCGACAT
TGGATAGGAACTGAG
TGGGTAATGTTACAC
TGGCTAGCCACTGAG
TGCTTCTAGATTGCT
TGCATTGTTACTCAC
TGCGTATAGGAAGCA
TGCCTACAAAGCTAG
TCTTTTAACATAGGA
TCTATAGCGAGACTG
TCTGTTTACTTACTG
TCTCTAGCCAGACAC
TCATTTGAGAAACTC
TCAATACTCTGCTTG
TCAGTTTAGACAGGA
TCACTACAGAGGAAG
TCGTTCGAGACTGTT
TCGATAGTGAGGAAC
TCGGTTGACATAGGT
TCGCTTGTTACATAG
TCCTTCCTGTTAGAA
TCCATACAGAGCCAG
TCCGTCTACAAACAT
TCCCTAGGAAGCCAG
ATTTTCGTGCGTGTG

b

TTTATTGTGAAAC
TTTGTAGAATGTT
TTTCTACAAACTC
TTATTAGAAAGAT
TTAATTGTTACAT
TTAGTAGCCTGTT
TTACTACATAGGT
TTGTTAGGAAGCG
TTGATAGGCTGTT
TTGGTACATAGGT
TTGCTAGTAACAT
TTCTTTGTTAGCC
TTCATACAAACTG
TTCGTTGTTAGAG
TTCCTAGTAACAT
TATTTAGAATGTT
TATATACACAGTA
TATGTACTCTGTT
TATCTAGGAAGCG
TAATTTGTTAGCC
TAAATACAAACTG
TAAGTTGTTACTC
TAACTACATAGTA
TAGTTACTGACTC
TAGATTGCGTGTT
TAGGTATCGAGCC
TAGCTACACTGTT
TACTTACACAGAA
TACATTGTTAGGC
TACGTAGCGAGCC
TACCTACACTGTT
TGTTTACATAGGT
TGTATAGTAACAT
TGTGTTGCTTGTT
TGTCTAGGAAGCG
TGATTTGTTAGCT
TGAATAGTAACTG
TGAGTAGACAGAA
TGACTTGTTAGCA
TGGTTAGAAAGTA
TGGATACTCACAA
TGGGTACTGAGAA
TGGCTTGCTTGTT
TGCTTAGCCACAA
TGCATACTGTGTT
TGCGTAGAGAGTA
TGCCTACATAGAA
TCTTTTGTTAGGA
TCTATACTCTGTT
TCTGTAGGAAGCG
TCTCTTGTTAGCC
TCATTACAAACTG
TCAATTGTTAGAC
TCAGTAGAAAGCG
TCACTAGAAACTC
TCGTTTGCGTGTG
TCGATTGTTTGCA
TCGGTTGTTATGG
TCGCTAGTAAGCA
TCCTTAGAAACTC
TCCATTGTTAAA
TCCGTCAGTAAC
TCCCTATACTCA
ATTTTGCCAGCG

Supplementary Figure 5 | 64 target sequences (distinct ID and feature sequences shown only, with common primer sequence omitted). a, 5-nt ID and 10–11-nt target feature sequences in the

synthesis work presented with Fig. 4. b, 5-nt ID and 7–8-nt target feature sequences in the synthesis work presented with Extended Data Figure 2.

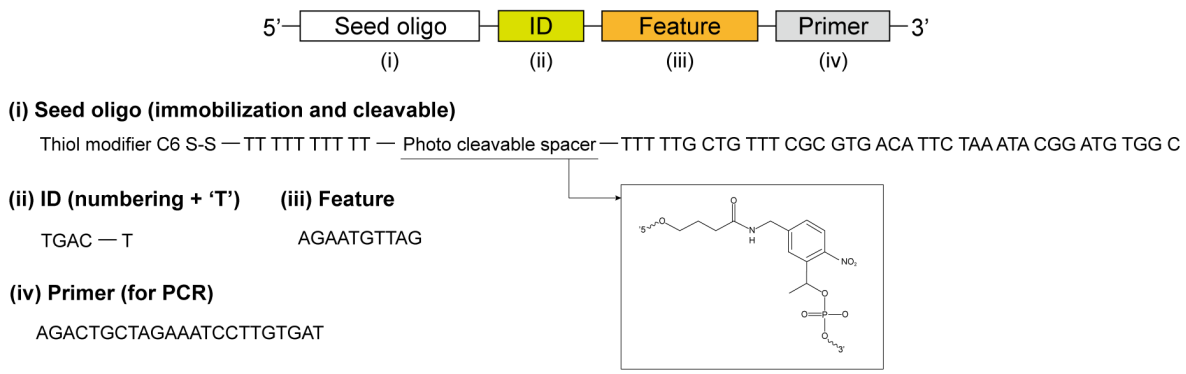

Supplementary Figure 6 | DNA sequence design. One of the 64 target sequences for the synthesis work of **Fig. 4** (5-nt ID, 10–11-nt feature, and 23-nt primer) is shown in full here together with the seed oligo sequence. The seed oligo (i) has a thiol modifier at its 5'-end for immobilization onto a pixel center gold electrode. The seed oligonucleotides have been modified with a photo-cleavable spacer (IDT PC Spacer, product no. 1707), which contains a nitrobenzyl-based photolabile group that is cleaved upon exposure to 365 nm UV light. This photolysis releases the DNA from the surface by breaking the bond between the thiol anchor and the oligo. Next, the ID sequence (ii), used to identify the pixel location of the sequence, always ends with base T to avoid G-quadruplex formation. The feature sequence (iii) contains the portion of the entire data to be synthesized at the pixel location designated by the ID sequence. Lastly, the primer sequence (iv) is synthesized to terminated at the 3′-end for PCR. Although this seed oligo immobilization scheme is designed for single-use only, it may be feasible to regenerate the gold surface by electrochemically stripping the thiol monolayer for re-immobilization.

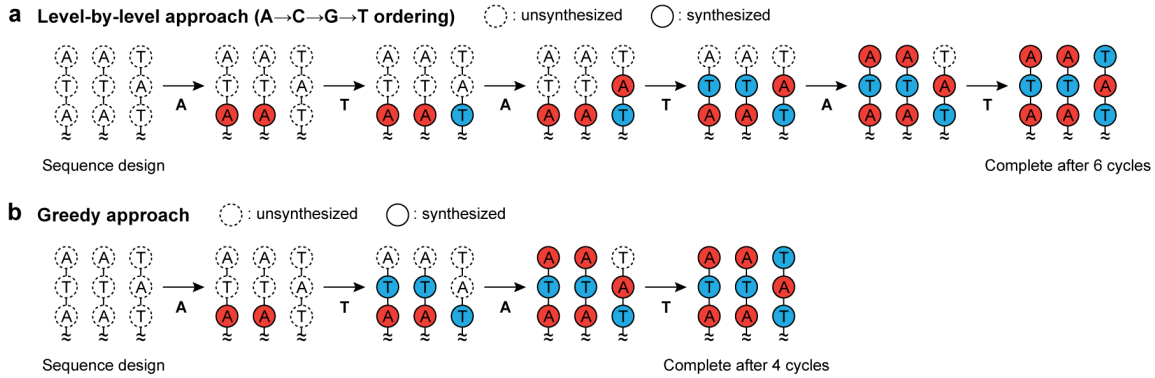

Supplementary Figure 7 | Level-by-level vs. greedy approaches for multi-sequence synthesis. An example to show how the greedy approach can reduce the number of synthesis cycles in multi-sequence synthesis as compared to the level-by-level approach. The level-by-level approach completes the synthesis at a given level before proceeding to the next level (part **a**). In contrast, in the greedy approach, at any given cycle, we choose the base type that has the largest number of destination pixels at all available levels, and activate these pixels to add nucleotides of that chosen base type at all available levels (part **b**).

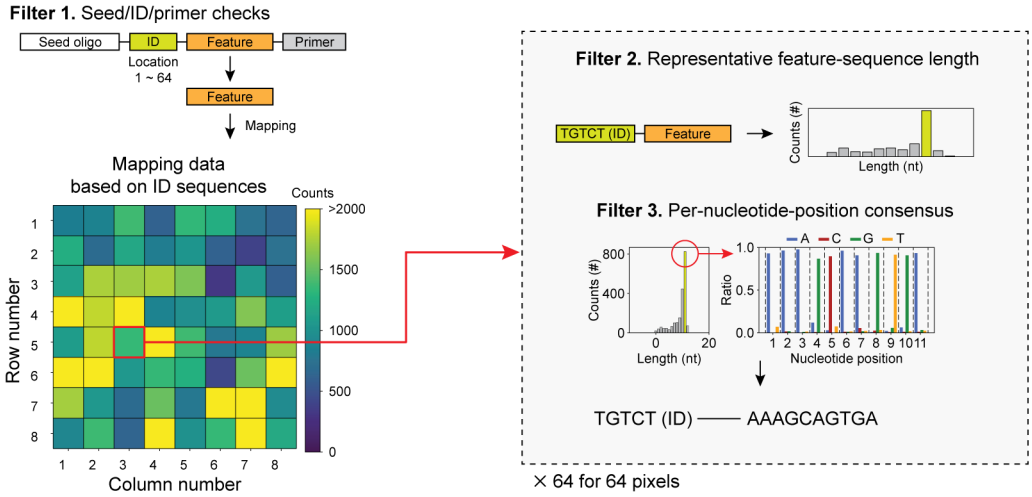

Supplementary Figure 8 | Filtering steps used for the analysis of the NGS reads in the case of the 64-sequence synthesis of Fig. 4. We filter out all NGS reads that do not have the correct combination of the seed oligo sequence, the ID sequences, and the primer sequence (there are 64 such combinations, since there are 64 distinct ID sequences, while the seed and primer sequences are common) (Filter 1). After Filter 1, the reads are classified into their pixel locations based on their ID sequences. Subsequently, the most frequent feature sequence length is identified as the representative length for each pixel position, and reads with feature lengths different from the representative length are filtered out (Filter 2). This approach ensures that sequence analysis is performed only on the majority-length products, which are presumed to reflect the intended synthesis outcome. This method ensures that synthesis errors (e.g., insertions or deletions) do not distort the overall sequence alignment and provides a practical solution to handling minor length variations. Next, at each pixel location, the most frequent base at each nucleotide position is identified among the reads with the representative length, and this forms the reconstructed consensus sequence (Filter 3).

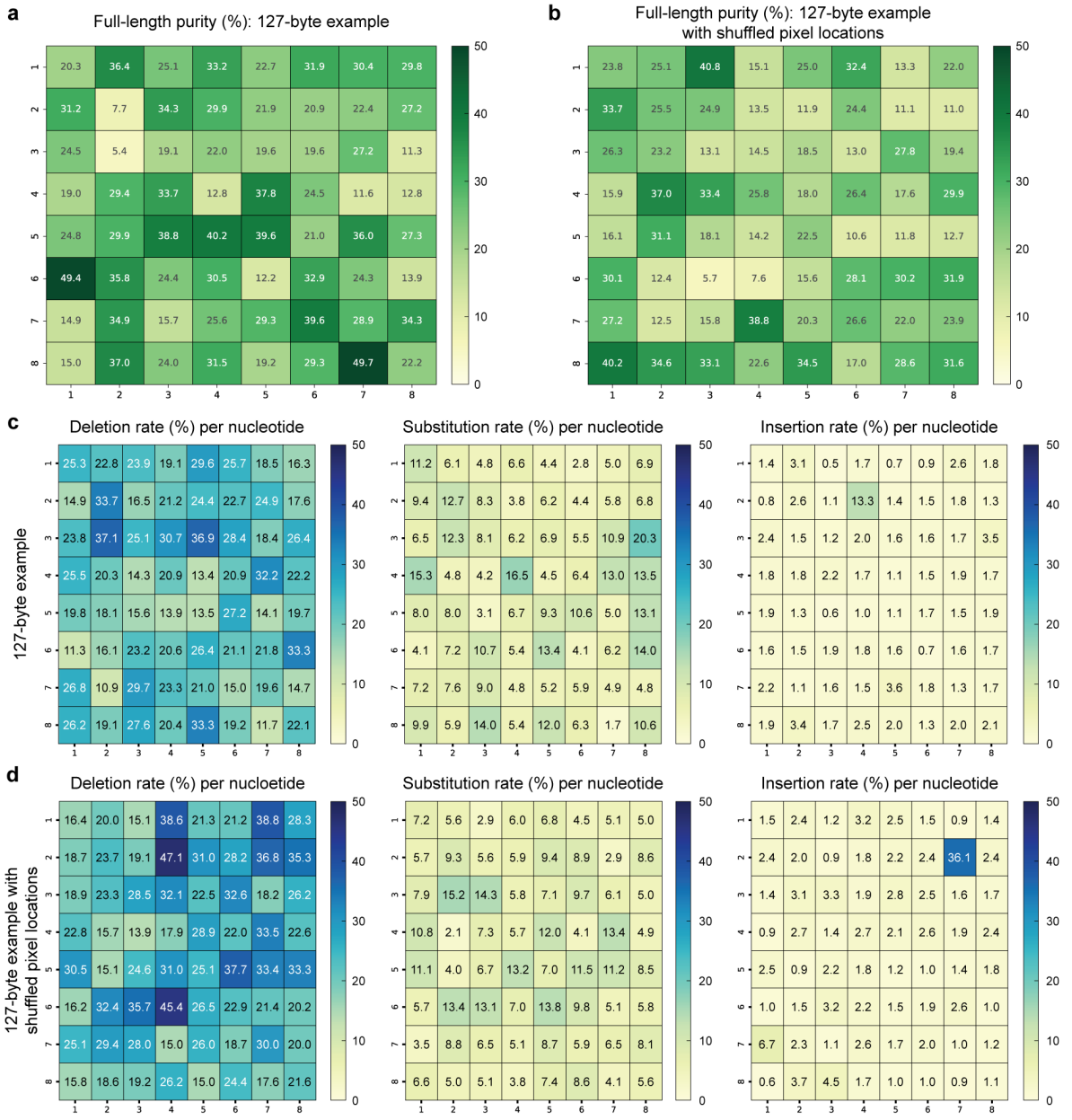

Supplementary Figure 9 | Pixel-resolved error maps for two runs of parallel 64-sequence synthesis (7–8-nt feature sequences). For experimental context and setup, see Extended Data Fig. 2. **a, c,** Pixel-by-pixel maps of full-length purity (panel **a**) and per-nucleotide error for deletions, substitutions, and insertions (panel **c**) for the second run in Supplementary Table 4. **b, d,** Pixel-by-pixel maps of full-length purity (panel **b**) and per-nucleotide error for deletions, substitutions, and insertions (panel **d**) for the third run in Supplementary Table 4. Between these two runs (**a, c** vs. **b, d**), the sequence-to-pixel assignments are shuffled.

```
def binary_to_dna(bin_data):
    mapping = {
        "01": "A",
        "00": "T",
        "11": "C",
        "10": "G"
    }
    return ''.join(mapping[bin_data[i:i+2]] for i in range(0, len(bin_data), 2))

def file_to_binary(filename):
    with open(filename, 'rb') as f:
        binary_data = ''.join(format(byte, '08b') for byte in f.read())
    return binary_data

def divide_sequence_evenly(sequence, num_sites):
    avg_segment_length = len(sequence) // num_sites
    remainder = len(sequence) % num_sites

    segments = []
    start = 0

    for i in range(num_sites):
        end = start + avg_segment_length
        if remainder > 0:
            end += 1
            remainder -= 1
        segments.append(sequence[start:end])
        start = end

    return segments

def number_to_dna(number):
    # Convert number to 8-bit binary representation
    bin_data = format(number, '08b')
    return binary_to_dna(bin_data)

def main():
    output_dna_filename = "path/dna_sequence_DNA_TEXT_169bytes_64sites.txt" #target text data
    site_number = 64  # Change this to the desired number of sites
    input_txt_filename = "path/DNA_sequences_169bytes.txt" #converted sequences

    # Convert text file to binary
    binary_data = file_to_binary(input_txt_filename)

    # Convert binary to DNA sequence
    dna_sequence = binary_to_dna(binary_data)

    # Divide the DNA sequence into specified number of sites
    dna_segments = divide_sequence_evenly(dna_sequence, site_number)

    # Save DNA sequence segments to a text file with fixed-width order number encoded as DNA
    with open(output_dna_filename, 'w') as f:
        for index, segment in enumerate(dna_segments, 1):  # Starts counting from 1
            order_dna = number_to_dna(index)
            f.write(order_dna + 'T' +segment + '\n') #'T' between numbering and data segment

    print(f"Encoded DNA sequence saved in {len(dna_segments)} segments in {output_dna_filename}")

if __name__ == "__main__":
    main()
```

Supplementary Figure 10 | Algorithm to encode binary data into DNA sequences. In this work, we use a simple algorithm that maps 01, 00, 11, and 10 to A, T, C, and G, respectively. We then break down the resulting sequence into multiple shorter feature (payload) sequences, and synthesize them, together with the ID and primer sequences, in parallel across many pixels.

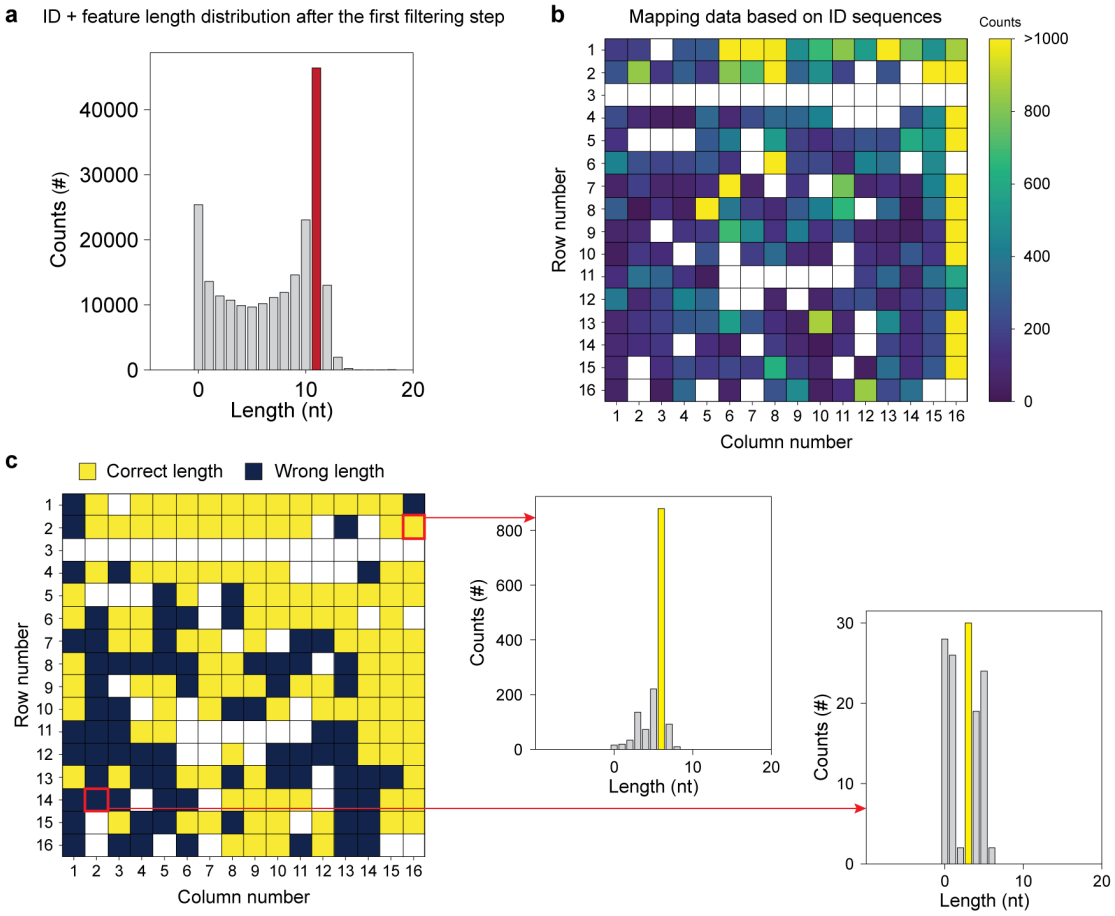

Supplementary Figure 11 | An attempt for multi-sequence synthesis using 200 pixels. In this example, we seek to synthesize 200 distinct sequences using 200 pixels, with each target sequence being 34-nt long (5-nt ID, 6-nt feature, and 23-nt primer); the remaining 56 pixels are unused due to suboptimal post-fabrications for the particular CMOS chip used here. **a,** In the analysis of the NGS reads of the synthesized DNA molecules, the ID + feature length distribution—collective distribution before assorting the NGS reads, which survive Filter 1, into their genesis pixel locations—shows that the most frequent length is indeed 11 nt as expected. **b,** However, the ID sequence-based assortment of the NGS reads into their genesis pixel locations shows that many pixels feature a very low number of reads (in the passing, note that blank pixels in the figure indicate the unused 56 pixels). **c,** Furthermore, in 39% of the 200 pixels used, representative feature lengths differ from the target feature length (6 nt).

a

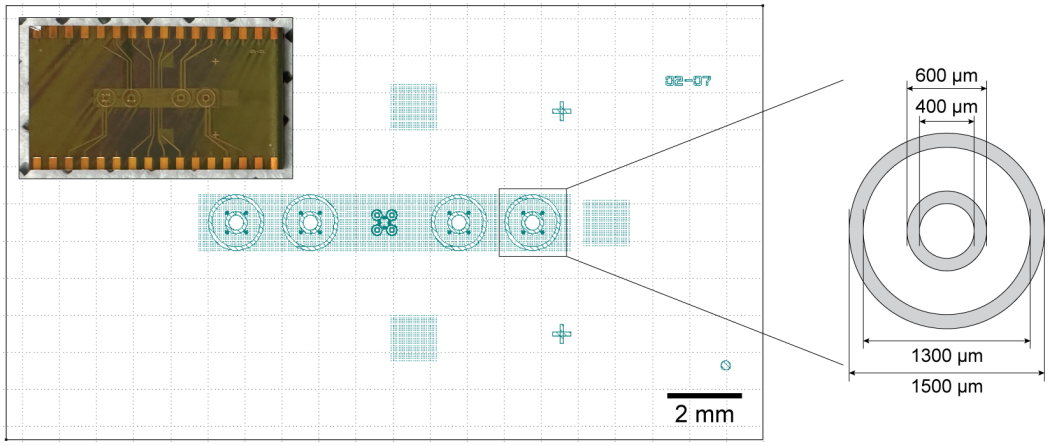

b

Multi-sequences

e13: 5'-GAA-CTT-CAA-CTT-CAA-CGG-CCT-3'

e8: 5'-AAT-GAT-CAA-GTT-CGG-AGA-CGT-3'

q4: 5'-GTC-TCT-GCG-GAG-GAA-GAC-ACT-3'

Fluorescence labelling

(Green) **t-e13-AF488**: 5'-TAGs-GCC-GTT-GAA-GTT-GAA-GTT-C-3'

(Red) **t-e8-Atto647N**: 5'-TAC-GTC-TCC-GAA-CTT-GAT-CAT-T-3'

(Orange) **t-q4-AF555**: 5'-TAG-TGT-CTT-CCT-CCG-CAG-AGA-C-3'

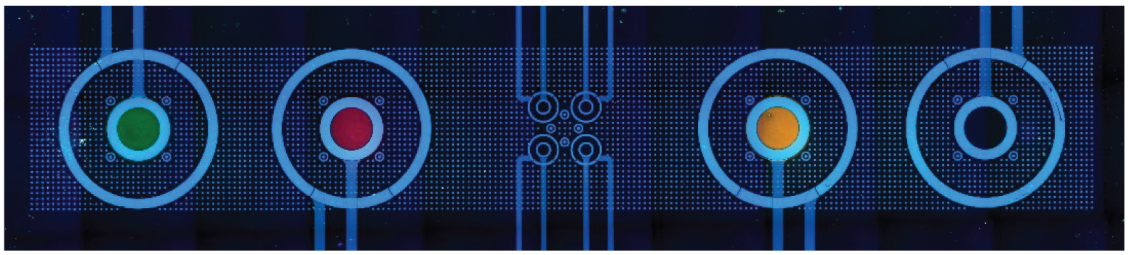

Supplementary Figure 12 | 4-pixel chip: synthesis studies. a, Layout of four ring-pair pixels arranged in two sets: 2 mm spacing within each set, and 4 mm spacing between sets. Electrode trace width is 200 μm. Seed oligos are immobilized within the inner ring. **b,** We performed a parallel three-sequence synthesis using two pixels from the left-side set and one pixel from the right-side set. The resulting fluorescence micrograph clearly shows three distinct 21-nt feature sequences (e13, e8, q4), hybridized to complementary probes labeled with AF488, Atto647N, and AF555, confirming successful synthesis of the three sequences. NGS data (Supplementary Table 6) further validate correct synthesis, and show that the two closer pixels yielded higher coupling efficiencies than the more distant pixel—opposite of what D2 (cross-pixel damage) would predict—, confirming negligible D2. We then used the 4-pixel chip for single-sequence synthesis of a 21–71-nt feature sequence, achieving 96.8–97.3% coupling efficiency (Supplementary Table 7).

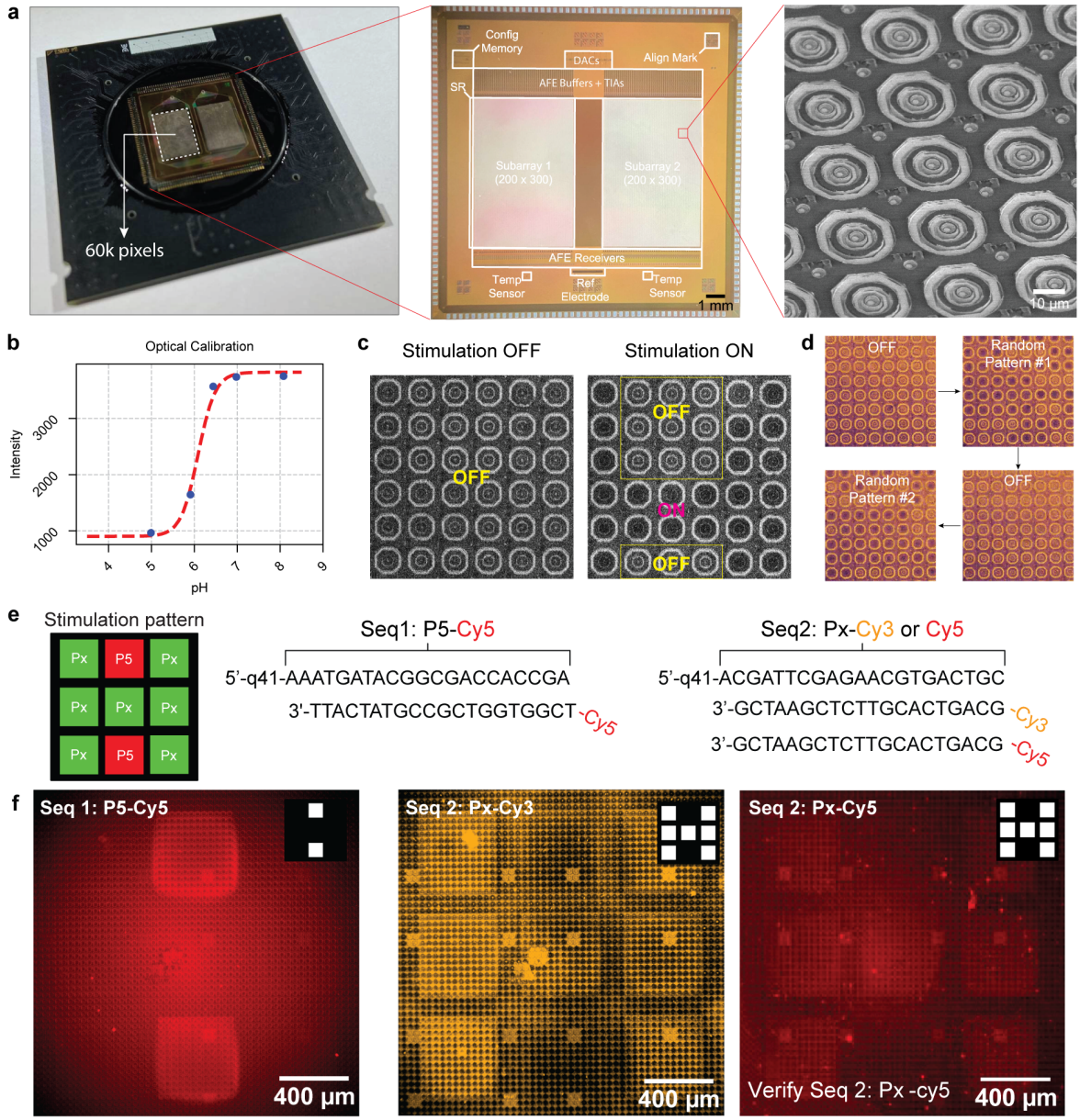

Supplementary Figure 13 | 120,000-pixel CMOS chip: synthesis studies. a, Photograph, layout (two 60,000-pixel subarrays, digital-to-analog converters (DACs), analog front end (AFE) receivers, and reference electrodes), and SEM image of ring-pair pixels. 32-μm pitch between ring-pair pixels. **b,** Optical calibration curve of pH-sensitive fluorophores. **c-d,** Fluorescence-based pH monitoring before/after stimulation and for random activation patterns, confirming pH localization at selected sites. Verification here is less comprehensive than on the main 256-pixel chip due to several suboptimal design features. Despite successful pH localization, which confirms hardware scalability, pixel-by-pixel synthesis fails, indicating strong D2 (cross-pixel damage) at this high density. **e,** Parallel synthesis scheme assigning two distinct sequences (P5 and Px) to different pixel blocks. Within active blocks, only anodic stimulation is applied across pixels; outside active blocks, only cathodic stimulation is applied across pixels. **f,** Fluorescence after hybridization, following synthesis. Cy5-labeled probes verify P5; Cy3/Cy5-labeled probes verify Px. Sequence formation is thus detected, but synthesis efficiency is very low and NGS was unsuccessful. This is consistent with: when a block is inactive, all of its pixels are inactive and D2 is reduced because any concurrently active pixels lie in other blocks that are, on average, more distant; when a block is active, substantial D1 and D2 remain.